# Millimeter-Wave Automotive Radar Scheme With Passive Reflector for Blind Corner Conditions

Dmitrii Solomitckii, Carlos Baquero Barneto, Matias Turunen, Markus Allén, Yevgeni Koucheryavy, Mikko Valkama
Tampere University, Tampere, Finland,
{dmitrii.solomitckii, carlos.baquerobarneto, matias.turunen, markus.allen, evgeny.kucheryavy, mikko.valkama}@tuni.fi

***Abstract*—One of the primary functions of millimeter-wave automotive radar is collision avoidance. This application is typically realized in line-of-sight conditions. However, it does not perform well in situations, when another car suddenly come into view around the corner of a building. Hence, this paper proposes a radar scheme with a reflector, enabling the detection of an oncoming car in blind corner conditions. First, our ray tracing modelling results demonstrate the difficulties of straightforward non-line-of-sight radar application in such a scenario. Then the paper considers the installation of a planar reflector, which should solve the issue. This is verified with real-world measurements. The results also indicate that the detection performance is sensitive to the around-the-corner car position and orientation of the reflector. Specifically, +/-10 degree deviation varies the signal-to-noise ratio of more than 20 dB. Thus, the location and direction of the reflector should be adopted individually for the particular deployment.**

***Index Terms*—mmWave automotive radar, electromagnetics, radio propagation, measurement.**

## I. Introduction

The introduction of new technologies (5G, machine learning, big data analysis, etc.), and the emergence of unmanned vehicles motivate the community to start developing advanced methods that enhance traffic safety. A vehicle should not only properly react to a threat, but also predict imminent, dangerous, driving situation. In addition, the ability of a vehicle *A* to detect an approaching vehicle *B* in non-line-of-sight (NLOS) conditions adequately fits into the objective above. Specifically, this is most relevant for urban crossroads, where a building may block the direct visibility between vehicles [1], [2]. Such condition is called *blind* or *blind corner* intersection.[1]

According to our literature review, the approaches for detecting objects behind an opaque wall are typically based on laser or radar. The laser-based approach employs combined action of the light beam and ultra-fast camera to capture a scattered field from a 3D object in NLOS conditions [3]–[6]. Despite the availability of LIDARs, which can be adopted for the task [7], the operation of the NLOS laser-based method in harsh outdoor environments is not well described in the current literature. It may be due to implementation problems or physical limits of the light associated with scattering and attenuation effects. Oppositely, radars are less sensitive to environmental conditions compared to lasers [8]. Many commercial cars [9] are already equipped with adaptive cruise control systems, where a millimeter-wave (mmWave) radar, operating at 77–80 GHz, plays a crucial role. One of its primary functions is collision avoidance. However, the line-of-sight (LOS) radar operation is limited in blind corner conditions, where another car may unexpectedly come into view around the building corner. Addressing the problem, this paper proposes the reflector-based NLOS radar scheme, which improves the detection performance in the blind corner intersection.

Broadly speaking, the around-the-corner or NLOS radar is not an original topic. For example, Rabaste et al. demonstrated the NLOS recognition of a human in a tunnel [10] and in a T-shaped room [11], by performing 2.5–3.5 GHz and 24 GHz radar measurements, respectively. A similar study was completed in [12], where a moving human being, hidden behind a concrete wall, was detected with a Doppler-based radar. The results in [13] demonstrate the micro-Doppler signatures of walking persons in the NLOS conditions (measured by a X-band radar). Nevertheless, all the aforementioned publications mainly focus on the NLOS radar-based detection/localization of a human without any manually-installed reflectors.

The most relevant study was completed in [14], where authors identified the moving vehicles in the NLOS conditions, using 10 GHz radar. These measurements were carried out in an urban environment, where the NLOS detection is feasible without any additional reflectors. In our paper, we consider a blind corner topology, where the NLOS or around-the-corner detection is extremely challenging.

The rest of the paper is organized as follows. Section II describes the scenario of interest in detail, while Section III specifies the methodology applied in this study. Specifically, it describes the ray tracing (RT) simulator, mmWave radar setup, and the list of parameters being utilized. Section IV presents the RT simulation and measurement results. Finally, conclusion and discussion about the practical implementation of the proposed radar scheme are given in Section V.

## II. Deployments of Interest

General view of the blind corner intersection is shown in Fig 1a. The scenario represents a small piece of the Manhattan

[1]It should be clarified that the building's corner made of brick and concrete, for instance, is almost opaque to radio frequency emissions and completely blocks optical (laser) irradiation. Thus, through-wall NLOS detection techniques are not considered in this paper.

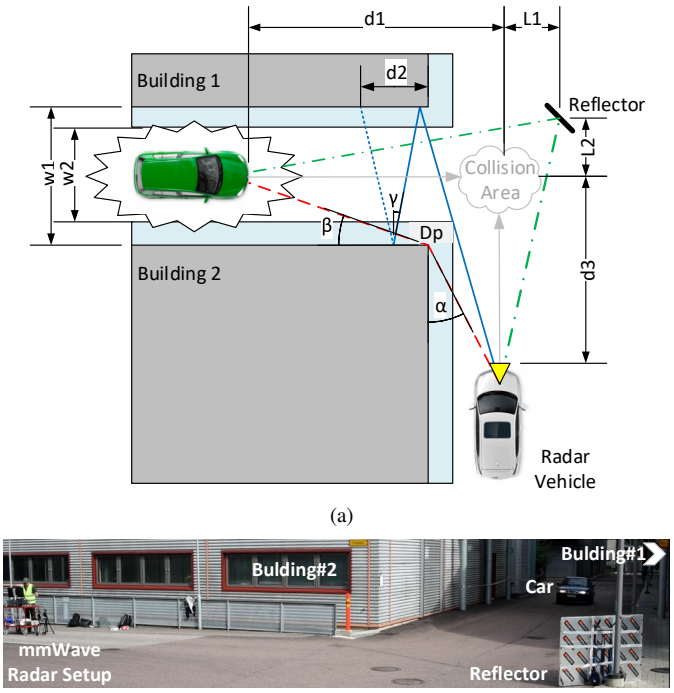


(a)




(b)

Fig. 1. The blind corner scenario employed in simulations (a) and the arrangement in the mmWave radar measurements (b).

grid, which mimics typical city layouts. It consists of a road surrounded by Building 1 and Building 2 on the sides. The light blue coloured zones are sidewalks. The detectable (green) car travels along the road with a certain speed, while the radar car (white) comes from behind the corner of the Building 2. The hypothetical collision area is determined as an intersection trajectories of these cars. The condition of the collision is the simultaneous presence of these cars in the collision area. This topology is utilized to carry out the measurements and to execute the simulations.

TABLE I
CONSIDERED SCENARIOS PARAMETERS

| Dimension | Simulated Scenario | Measured Scenario |
|---|---|---|
| d1 | 0...45 m | 0...45 m |
| d2 | max. 10 m | - |
| d3 | 10, 20, 30 m | 20 m |
| L1 | 3 m | 3 m |
| L2 | 3 m | 3 m |
| W1 | 7 m | 7 m |
| W2 | 5 m | 5 m |

*Measured deployment*. The real-world blind corner topology is identified in Hervanta Campus of Tampere University (see Fig. 1b) to carry out the mmWave radar measurements. The detectable car (Saab 9-3 OG, 2002) drives along the road, surrounded by Building 1 and Building 2. The car's speed is not exceeding 30 km/h for safety reasons. The walls of the buildings are covered with corrugated metal sheets. Moreover, the metal pipes (see Fig. 1b) are located next to the walls. It is assumed that such conditions may potentially contribute to the formation of the paths along which emitted and returned signals may propagate. Subsequently, it should adversely affect the functional performance of the NLOS radar [10]. Therefore, this particular area at Tampere University was selected as "challenging scenario" for our investigation. A constructional metallized foam-based insulator is employed to be the 1.2 x 1.8 m planar reflector (see "Reflector" in Fig. 1b). It is rigidly fixed to a heavy metal trolley to enable convenient transportation and reliable spatial orientation. The metallized insulator reflects the signal, emitting from the static mmWave radar setup, located at the distance of d3 = 20 m to the collision area. Other parameters of the measured deployment are listed in Table I.

*Simulated deployment*. The RT deployment represents a simplified 3D model of the measured deployment. Notably, the simplifications relate to the absence of metal objects and irregularities near/on the buildings. Similarly, the RT deployment consists of two cubical buildings, separated by the road, where the detectable car is assumed to drive. However, instead of the vehicle, the receiver's (RX's) route is placed along the road with the step of 0.1 m. The transmitters (TXs) are located behind the Building 2 at a distance d3 of 10, 20 and 30 m to the collision area. The material of the buildings is flat metal, with the reflecting coefficient $|\Gamma| = 1$. More detailed information is given in Table I.

## III. METHODOLOGY

In this paper, measurement and simulation methodologies are exploited. Each of them is described below.

### A. mmWave Radar Setup

Radar measurements are carried out based on the mmWave radar prototype described in our recent work [15]. In these experiments, we have adopted a separated TX-RX antenna configuration in order to improve the isolation between transmitter and receiver chains. A vector signal transceiver (VST) implements the RF TX and RX functionalities at intermediate frequency (IF) of 3.5 GHz which properly suits to the characteristics of filters installed in the setup. In addition, two signal generators are used as local oscillators to up-convert the IF signal to 28 GHz carrier frequency. The modulated OFDM signal is fed to the Pasternack PE9851A-20 transmitter horn antenna which provides a gain of 20 dBi with a beam width of 17°. The different reflections are then collected by a second identical horn antenna with a separation of 20 cm with respect to the transmitter. Both antennas were installed on two tripods with a height of 70 cm in order to simulate a vehicular radar system mounted on a car's bumper.

In the measurements, different OFDM waveforms with carrier bandwidths of 50, 100, 200 MHz and 60 kHz subcarrier spacing are employed. For all the analyzed configurations, a fixed signal duration of 10 ms is considered, which implies the same radar velocity resolution for all the cases. For the radar processing, we adopt subcarrier-domain processing utilizing directly the transmit and receive grids of samples similar to [16].

Signal-to-noise ratio (SNR) is the primary parameter of interest in the mmWave radar measurements. Thus, based on

the measured received power $P_\mathrm{r}$, the SNR can be obtained by the following formula:

$$SNR = \frac{P_\mathrm{r}}{P_\mathrm{n}} = \frac{P_\mathrm{r}}{kT_0FB}, \quad (1)$$

where $k \approx 1.38 \cdot 10^{23}\,\mathrm{W \cdot s/K}$ is Boltzmann constant, $T_0 = 290\,\mathrm{K}$ is the standard temperature, $B = 50, 100, 200\,\mathrm{MHz}$ is the instantaneous bandwidth, and $F$ = 15 is the noise factor. Accordingly, the noise levels for these bandwidths are −82, −79 and −76 dBm. Additional postprocessing gain is applied to calculate the SNR. It is expressed as $G = 10\log_{10}(S \cdot R)$, where $S$ and $R$ denote the number of subcarriers and OFDM symbols used in the radar processing, respectively.

### B. Ray Tracing Simulator

In this work, a simplified in-house built 2D RT is utilized. It mimics the multipath propagation channels in a site-specific environment. The first stage of the RT verifies, preprocesses and converts the 3D model of the deployment into the input data structure. Next, the geometrical engine searches the TX-RX propagation paths using the image method. As soon as all the paths are found, the physical stage specifies each of them by the electric (*E*-) and magnetic (*H*-) fields calculated by geometrical optics (GO) and uniform theory of diffraction (UTD) [17]. Finally, these electromagnetic fields are converted into the total received power metric, using the following equation [18]:

$$P_\mathrm{rx}[\mathrm{dBm}] = 10\log_{10}\left(\frac{\lambda^2|E|^2}{8\pi Z_0}\right) + G_\mathrm{tx} + G_\mathrm{rx} + P_\mathrm{tx}, \quad (2)$$

where $E$ is a complex signal, $P_\mathrm{tx} = 0\,\mathrm{dBm}$ is transmitted power, $G_\mathrm{tx} = 20\,\mathrm{dBi}$ and $G_\mathrm{rx} = 20\,\mathrm{dBi}$ are TX and RX gains, $\lambda$ is a wavelength 0.01 m, and $Z_0$ is the free-space impedance $120\pi\,\Omega$. The simulator settings are configured to perform 6 reflections and 1 diffraction.

## IV. Results

The results are divided into two groups: simulated by the RT and measured by the mmWave radar setup. Each of them is described below in detail.

### A. RT modelling

The RT modelling is performed to investigate the underlying propagation paths in the blind corner conditions. For this purpose, calculation of the received power and the number of multipath components (MPCs) (contributing this power), at the RX route is executed. It is suggested that if the received power at the RX route exceeds the noise level, then the return signal can theoretically be captured. If the received power is below the noise floor, then a calculation of the return signal is meaningless, since it is strictly below the noise level. Such simplistic analysis may help to understand the capability of the transmitted signal to reach the detectable car in the blind corner topology.

Fig. 2 shows the RT simulation results of the received power at different d1 (see Fig. 1a) and three TX positions

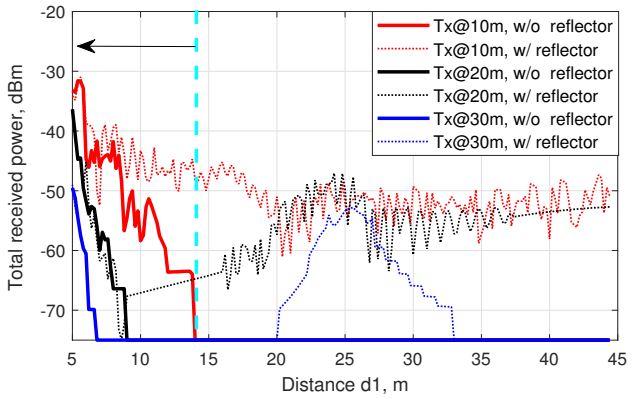


Fig. 2. The total received power as a function of distance d1 and d3.

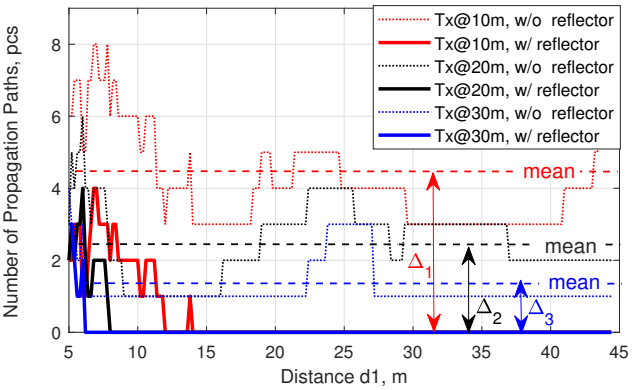


Fig. 3. The number of MPCs as a function of distance d1 and d3.

d3. When the reflector is not employed (solid lines in Fig. 2), the received power is consistently below the noise floor at d1 $>$ 14 m (cyan dashed line in Fig. 2). Moreover, the cyan dashed line begins shifting to zero (see black arrow), as soon as the TX moves away from the collision area (e.g., d3 increases). Fig. 3 is plotted to explain the total received power behaviour. Following this, there is no single path at d1 $>$ 14 m (solid red line) that could somehow potentially contribute to the total received power. Although the two primary propagating paths (diffracting red and reflecting blue in Fig. 1a) are available, they are entirely useless in the blind corner intersection. First, the diffraction path has minimal angles $\alpha$ and $\beta$, which lead to a significant one-way loss above 30 dB [19]. Meanwhile, the high order reflection (blue line in Fig. 2) is posed as an alternative propagation path. However, due to the small angle of incidence $\gamma$, the transmitting signal cannot propagate deep along the road. The propagation distance d2 $<$ 15 m, and this mechanism contributes the most to the total RX power in Fig. 2, when there is no reflector (solid lines). It is also worth noting that when the signal impinges on a real-world dielectric wall at the small $\gamma$, the reflection losses are close to maximum, and, thus, the signal attenuates fast.

Furthermore, all the previous simulations are repeated for the same deployment with metallic planar reflector. As a result, this improvement increases the number of MPCs shown in

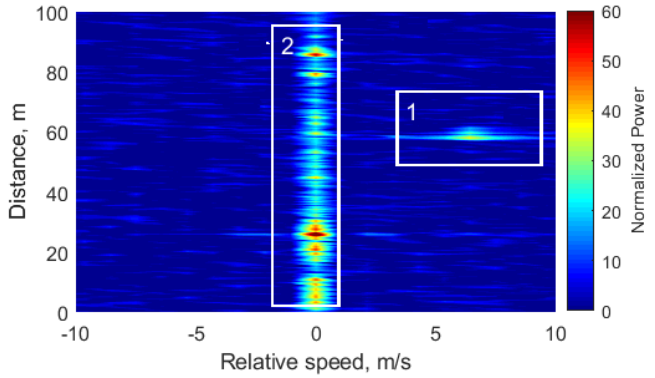


Fig. 4. Measured power profile by the mmWave radar setup. The scattered signal from the car, driving in the center of the road, is shown in Rectangle 1. The velocity of the car is 6.5 m/s while signal BW is 200 MHz.

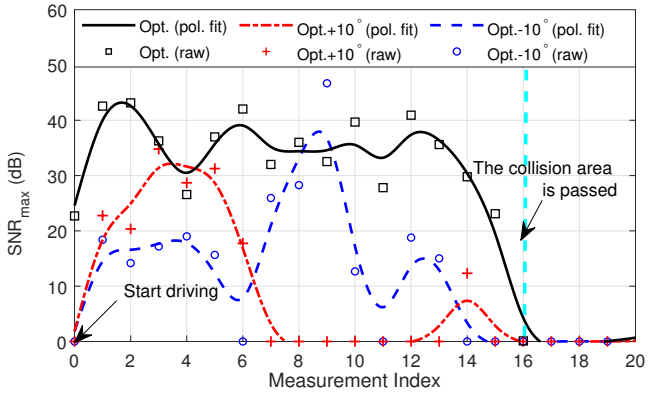


Fig. 5. The influence of the reflector rotation on the maximum SNR. The car drives in the center of the road, signal BW is 200 MHz. Markers represent raw data, while solid lines demonstrate the markers polynomial fit.

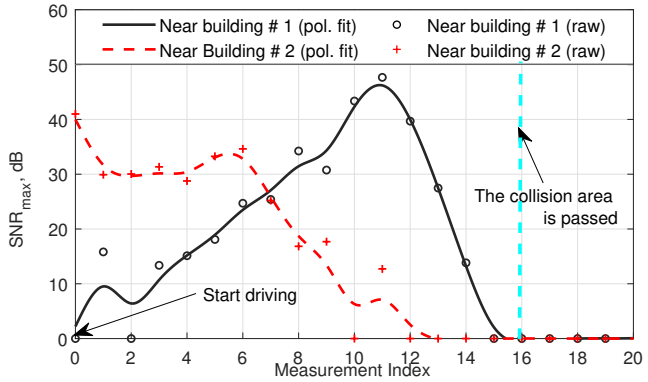


Fig. 6. Effect of the car position on the detection capability. Signal BW is 200 MHz, and the reflector angle is optimal. Markers represent raw data, while solid lines demonstrate the markers polynomial fit.

Fig. 3, while the total received power becomes higher than the noise floor even at d1 $>$ 15 m (dashed lines). The reflector creates, on average, 2–4 new MPCs. Nevertheless, when the distance d3 changes, the pattern of the total received power modifies accordingly. Moreover, rising of the distance d3 reduces the efficiency (the number of generating paths) of the reflector proportionally ($\Delta_1 > \Delta_2 > \Delta_3$ in Fig. 3). Only the RXs located between d1 = 20…35 m may receive a signal above the noise floor at d3 = 30 m (see Fig. 2). This suggests that the relative position of the TX and RX greatly affects the detection capability.

### *B. Measurement*

This section reveals the measurement results of the blind corner area in Tampere University. More precisely, a proof-of-concept as well as the sensitivity analysis of the detection capability are presented.

Continuously measured 20 snapshots of the power profile are collected during the car driving. Fig. 4 demonstrates one of the 20 captured power profiles, where the white Rectangle 2 denotes static objects, and Rectangle 1 highlights the moving car. All subsequent figures (Figs. 5, 6 and 7) are derived based on the maximum power inside the Rectangle 1.

The first set of measurements is completed without a reflector. In this case, the mmWave radar is unable to recognize the upcoming car, i.e. Rectangle 1 in Fig. 4 was entirely blue. After this, rough placement (approx. 40°) of the reflector is attempted, resulting in the immediate detection of the return signal from the car. Following this, the next task is to find the optimal angle, when the detection performance is the best, i.e. the SNR value of the returned signal is the highest. For that purpose, nine measurements are carried out, where the orientation of the reflecting plane was changing by 10° steps from 0° to 90°. As a result, the optimum angle of 30° is revealed. Based on the measured results in Fig. 5, deviation from the optimum by ±10° reduces the average SNR more than 20 dB. Furthermore, a rotation of more than ±10° reduces the SNR almost to zero. Consequently, it can be argued that the installation of a flat planar reflector should be carried out with an accuracy of ±10°, to guarantee functional detection capabilities. Such precise installation, potentially, may require the utilization of specific adjusters.

The next step is the analysis of the detection sensitivity to the car position. For this purpose, two scenarios are considered: when the car drives as close as possible to Building 1 or Building 2. The results are shown in Fig. 6. In the first case, the driving car reflects the highest signal when the distance to the collision area d1 is small (black line in Fig. 6). Oppositely, the car moving next to Building 2 (red line in Fig. 6) contributes the highest SNR being at a considerable distance d1. So, it can also be claimed that the detection performance of the scheme with a reflector is highly dependent on the position of the car relative to the surrounding buildings.

The final task is to determine how the bandwidth affects the SNR. From the radar theory point of view, the bandwidth affects the ability to distinguish details of one object or to identify multiple ones. According to measurement results being plotted in Fig. 7, this assumption is confirmed. Additionally, it can be argued that reliable detection of a car, driving in the blind corner conditions, is feasible even with $B = 50$ MHz. However, based on the practical observations being done during the measurements, the recognition of several objects needs at least $B = 100$ MHz.

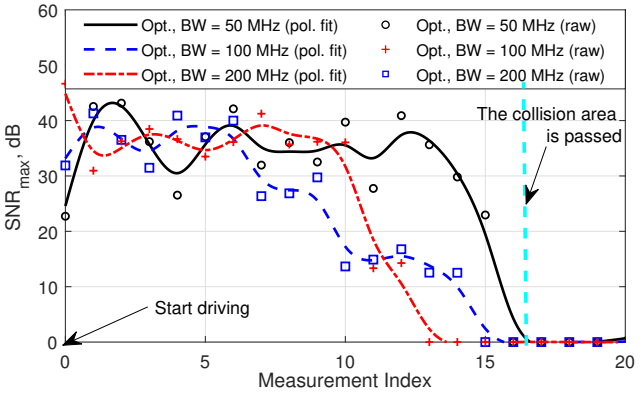


Fig. 7. Effect of bandwidth on the detection capability. The car drives in the center of the road and the reflector angle is optimal. Markers represent raw data, while solid lines demonstrate the markers polynomial fit.

## V. Conclusion

In this article, we demonstrated the operation of the automotive mmWave radar scheme with a planar reflector in blind corner conditions. First, the RT simulation results explained the underlying geometrical paths, along which transmitted and received signals propagate around the corner. Then, the mmWave radar measurement was carried out to show the practical feasibility and operational reliability of the proposed scheme. Based on the work done, the following findings are made. The radars indeed may detect in the NLOS conditions. However, not every topology supports this. Specifically, it was shown that in the blind corner conditions, which is the essential part of an urban topology, such detection looks challenging due to geometrical and physical reasons. However, mounting of the reflector may resolve the problem.

Nonetheless, there are number of improvements that should be addressed to guarantee an efficient operation of the mmWave radar reflector scheme:

- *Small reflector's size*. The main task is to find the optimal size performing the best detection probability in a particular environment. Potentially, the accurately selected shape may minimize the size of the reflector.
- *Seamless coverage in NLOS*. Conceivably, the matrix of passive reflectors or multilayered scattering coating may enhance the transmission to the NLOS region. Additionally, the properly selected geometry and size may also contribute to it.
- *Weak effect of dust and dirt.* Obviously, the finely dispersed layer on the reflector's surface affects the reflection and diffuse scattering coefficients at the mmWave. A potential solution to this problem may be applying a layer with a large contact angle of wetting [20].

All the improvements mentioned above will be investigated in the following studies.

## VI. Acknowledgment

This work was partially supported by the Academy of Finland (grant #319994).

## References

[1] Y. Yoshihara, Y. Morales, N. Akai, E. Takeuchi, and Y. Ninomiya, "Autonomous predictive driving for blind intersections," in *2017 IEEE/RSJ International Conference on Intelligent Robots and Systems (IROS)*, Sep. 2017, pp. 3452–3459.

[2] Y. Morales, Y. Yoshihara, N. Akai, E. Takeuchi, and Y. Ninomiya, "Proactive driving modeling in blind intersections based on expert driver data," in *2017 IEEE Intelligent Vehicles Symposium (IV)*, Jun. 2017, pp. 901–907.

[3] V. Arellano, D. Gutierrez, and A. Jarabo, "Fast back-projection for non-line of sight reconstruction," *Optics express*, vol. 25, no. 10, pp. 11 574–11 583, May 2017.

[4] G. Musarra, A. Lyons, E. Conca, Y. Altmann, F. Villa, F. Zappa, M. Padgett, and D. Faccio, "Non-line-of-sight three-dimensional imaging with a single-pixel camera," *Phys. Rev. Applied*, vol. 12, Jul. 2019.

[5] X. Liu, I. Guillén, M. La Manna, J. H. Nam, S. A. Reza, T. H. Le, A. Jarabo, D. Gutierrez, and A. Velten, "Non-line-of-sight imaging using phasor-field virtual wave optics," *Nature*, vol. 572, no. 7771, pp. 620–623, Aug. 2019.

[6] M. O'Toole, D. B. Lindell, and G. Wetzstein, "Confocal non-line-of-sight imaging based on the light-cone transform," *Nature*, vol. 555, no. 7696, pp. 338–341, Mar. 2018.

[7] A. Kirmani, T. Hutchison, J. Davis, and R. Raskar, "Looking around the corner using transient imaging," in *2009 IEEE 12th International Conference on Computer Vision*, Jul. 2009, pp. 159–166.

[8] P. F. McManamon, *LiDAR Technologies and Systems*. SPIE, 2019.

[9] K. Mays, "Which cars have self-driving features for 2019?" May 2019. [Online]. Available: https://www.cars.com/articles/which-cars-have-self-driving-features-for-2019-402645/

[10] O. Rabaste, E. Colin-Koeniguer, D. Poullin, A. Cheraly, J.-F. Pétex, and H.-K. Phan, "Around-the-corner radar: detection of a human being in non-line of sight," *IET Radar, Sonar & Navigation*, vol. 9, no. 6, pp. 660–668, Jun. 2015.

[11] T. Khac-Phuc-Hung, O. Rabaste, J. Bosse, D. Poullin, I. Hinostroza, T. Letertre, T. Chonavel *et al.*, "Around-the-corner radar: Detection and localization of a target in non-line of sight," in *2017 IEEE Radar Conference (RadarConf)*, Jun. 2017, pp. 0842–0847.

[12] A. Sume, M. Gustafsson, M. Herberthson, A. Janis, S. Nilsson, J. Rahm, and A. Orbom, "Radar detection of moving targets behind corners," *IEEE Transactions on Geoscience and Remote Sensing*, vol. 49, no. 6, pp. 2259–2267, Jan. 2011.

[13] M. Gustafsson, Å. Andersson, T. Johansson, S. Nilsson, A. Sume, and A. Örbom, "Extraction of human micro-doppler signature in an urban environment using a sensing-behind-the-corner radar," *IEEE Geoscience and Remote Sensing Letters*, vol. 13, no. 2, pp. 187–191, Dec. 2015.

[14] T. Johansson, A. Örbom, A. Sume, J. Rahm, S. Nilsson, M. Herberthson, M. Gustafsson, and Å. Andersson, "Radar measurements of moving objects around corners in a realistic scene," in *Radar Sensor Technology XVIII*, vol. 9077, May 2014.

[15] C. Baquero Barneto, M. Turunen, S. Liyanaarachchi, L. Anttila, A. Brihuega, T. Riihonen, and M. Valkama, "High-accuracy radio sensing in 5G New Radio networks: Prospects and self-interference challenge," in *Proc. Asilomar Conf. Signals, Syst., Computers (ASILOMAR)*, Nov. 2019.

[16] M. Braun, "OFDM radar algorithms in mobile communication networks," Ph.D. dissertation, Karlsruhe Institute of Technology, Jan. 2014.

[17] D. McNamara, C. Pistorius, and J. Malherbe, "The uniform geometrical theory of diffraction," *Artech House, London*, 1990.

[18] D. Solomitckii, V. Semkin, A. Karttunen, V. Petrov, S. Le Hong Nguyen, H. Nikopour, K. Haneda, S. Andreev, S. Talwar, and Y. Koucheryavy, "Characterizing radio wave propagation in urban street canyon with vehicular blockage at 28 GHz," *IEEE Transactions on Vehicular Technology*, Jan. 2020.

[19] S. Deng, G. R. MacCartney, and T. S. Rappaport, "Indoor and outdoor 5g diffraction measurements and models at 10, 20, and 26 GHz," in *2016 IEEE Global Communications Conference (GLOBECOM)*, Dec. 2016, pp. 1–7.

[20] Y.-Y. Quan, L.-Z. Zhang, R.-H. Qi, and R.-R. Cai, "Self-cleaning of surfaces: the role of surface wettability and dust types," *Scientific reports*, vol. 6, p. 38239, Dec. 2016.